Colloids and Surfaces B: Biointerfaces 191 (2020) 110984

Contents lists available at ScienceDirect

Colloids and Surfaces B: Biointerfaces

journal homepage: www.elsevier.com/locate/colsurfb

Synthesis of water soluble $CuGaS_2$/ZnS quantum dots for ultrasensitive fluorescent detection of alkaline phosphatase based on inner filter effect

Xiaoxia Huangfu[1], Yang Shen[1], Anzi Yang, Lixiao Liu, Wen Luo, Wenbo Zhao*

National and Local Joint Engineering Research Center of Biomedical Functional Materials, School of Chemistry and Materials Science, Nanjing Normal University, Nanjing, 210023, China

ARTICLE INFO

Keywords:
GSH-$CuGaS_2$/ZnS QDs
Water solubility and biocompatibility
Fluorescent detection
Alkaline phosphatase
Inner filter effect

ABSTRACT

Developing monitoring technique for alkaline phosphatase (ALP) is crucial due to the important role it plays in living cells. Here, a kind of biocompatible glutathione-modified $CuGaS_2$/ZnS quantum dots (GSH-CGS/ZnS QDs) was used as a fluorescent substance and then fabricated "turn-off" fluorescent biosensor for detection of ALP by help of inner filter effect (IFE). Firstly, we prepared $CuGaS_2$/ZnS (CGS/ZnS) QDs using solvothermal method and explored the efficient ligand (GSH) exchanges strategy for transferring oil-soluble CGS/ZnS QDs to aqueous phase. More importantly, we also explored the potential biological applications of the nanohybrid QDs. The obtained GSH-CGS/ZnS QDs emitted strong yellow fluorescence with the maximum excitation (400 nm) and emission (601 nm). Then, GSH-CGS/ZnS QDs were mixed with p-nitrophenylphosphate (PNPP) and ALP. PNPP could be hydrolyzed to p-nitrophenol (PNP) by help of catalysis of ALP, and the excitation spectrum of the GSH-CGS/ZnS QDs overlapped well with the absorption spectrum of PNP, so the fluorescence of GSH-CGS/ZnS QDs was initially quenched *via* the so-called "IFE". Finally, a novel "turn-off" biosensor for sensitive detection of ALP in the range of 0.05–10 U L^{-1}(R^2 = 0.98) with a detection limit of 0.01 U L^{-1} was successfully obtained. Results indicated that I-III-VI_2 nanocrystals have great potential for their promising biomedical application.

1. Introduction

Over the past years, quantum dots (QDs) are very promising semiconductor nanomaterials due to their excellent optical properties. Unlike those traditional organic dyes, QDs show unique advantages in biological applications, such as bright and size-tunable fluorescence properties, resistance to photobleaching and large stokes shift [1–4]. However, most of semiconductor nanocrystals are toxic which has limited their clinical application in the biological field [5–8]. Many researchers have confirmed that these toxic compounds can be degrade and released into the human body environmental. For this reason, the cadmium (Cd)-free QDs based on III-V or I-III-VI_2 materials has been actively studied [9,10].

Recently, the solvothermal method and hot injection techniques have been adopted to synthesis I-III-VI_2 QDs. Ternary group I-III-VI_2 semiconductor materials include $AgInS_2$ [11], $CuInS_2$ [12] and $CuInSe_2$ [13] have been widely investigated. These materials have tunable emission and less toxicity, which make them promising alternatives for biological field [14,15]. To date, many interesting $CuGaS_2$ nanostructures have been designed and prepared by different methods [16–24]. Yang et al. reported the synthesis of non-Cd core/shell structural CGS/ZnS QDs with strong photoluminescence (PL) emission, and investigated their application for lighting source [24]. Despite of many achievements from these studies, most of the researches focused on lighting source or solar energy conversion of $CuGaS_2$ nanomaterials. To the best of our knowledge, the $CuGaS_2$ QDs are rarely used in biological applications due to their weak fluorescent properties and hydrophobic surface. Therefore, it is important to synthesize water-soluble $CuGaS_2$ QDs with good fluorescence properties for biomedical applications.

Alkaline phosphatase (ALP) is regarded as an important indicator for many diseases, including breast cancer, bone disease and liver disease [25–27]. Recently, ALP enzyme activity has been analyzed by several methods, such as colorimetric [28], chemiluminescence (CL) [29] and surface enhanced Raman scattering (SERS) [30–32] methods. However, these methods have some drawbacks such as high toxicity and complicated instruments, which limits their practical application. Therefore, it is necessary to find a facile and nontoxic way for sensitive

* Corresponding author at: National and Local Joint Engineering Research Center of Biomedical Functional Materials, Jiangsu Key Laboratory of Biofunctional Materials, Nanjing 210023, China.
E-mail address: zhaowenbo@njnu.edu.cn (W. Zhao).
[1] These authors contributed equally to this work.

https://doi.org/10.1016/j.colsurfb.2020.110984
Received 11 October 2019; Received in revised form 16 March 2020; Accepted 18 March 2020
Available online 19 March 2020

detection of ALP. Fluorescence assay has attracted much attention because of simplicity, short detection time and high sensitivity [33,34]. In this work, we prepared the CGS/ZnS QDs (Cu/Ga = 1/1) based on previously reported and slightly changed the synthetic path to obtained more uniform nanoparticles. Then, we transferred CGS/ZnS QDs from the organic phase to water phase by ligand exchange with 3-mercaptopropionic (MPA) and GSH for the first time [35]. After phase transfer, the obtained GSH-CGS/ZnS QDs were hydrophilic and their good fluorescence property was maintained (maximum excitation (400 nm) and emission (601 nm)), and then they were employed to prepare "turn-off" fluorescent biosensor for ALP analysis based on inner filter effect (IFE) [36]. In our case, when ALP was introduced, p-nitrophenylphosphate (PNPP) was hydrolyzed to p-nitrophenol (PNP) whose absorption spectra overlapped well with the excitation spectra of the prepared GSH-CGS/ZnS QDs, so the fluorescence of GSH-CGS/ZnS QDs was initially quenched by PNP, this process was called "IFE". Due to IFE, the fluorescence intensity of GSH-CGS/ZnS QDs was obviously weakened. Based on this strategy, a "turn-off" sensor for sensitive detection of ALP was developed successfully.

2. Materials and methods

2.1. Materials

Gallium(III) nitrate hydrate ($Ga(NO_3)_3{\cdot}xH_2O$, 99.99 %), cupric acetate anhydrous ($Cu(Ac)_2$), ≥98 %), oleylamine (OLA, 90 %), 1-octadecene (ODE, 90 %), Sublimed sulfur (S, 99.5 %), 3-mercaptopropionic (MPA, 99 %) and *N,N*-dimethylformamide (DMF, ≥99.9 %) were obtained from Aladdin. Oleic acid (OA, 90 %) and L-glutathione reduced (GSH, 98 %) were purchased from Sigma-Aldrich. N-dodecanethio (DDT) was available from Shanghai Lingfeng Co., Ltd. 3-(4,5-dimethylthiazolyl-2)-2,5-diphenyltetrazolium bromide (MTT) was acquired from Sangon Biotech (Shanghai) Co., Ltd.

2.2. Apparatus and measurements

The fluorescence spectra were collected with a fluorescence spectrophotometer (Hitachi F-4600) equipped with an excitation source of Xenon lamp. The UV/Vis spectra were obtained from a spectrophotometer (Varian Cary 50). The morphologies and size of QDs were characterized by transmission electron microscopy (TEM, HITACHI H-7650, 120 kV). X-ray diffraction (XRD) measurements were recorded on a Bruker D8 Advance X-ray diffractometer with Cu Kα (λ = 1.5418 Å). The fourier transform infrared (FTIR) spectra were obtained on a Bruker Vector 22 FTIR in the range of 400–4000 cm^{-1} using KBr pellets. Energy dispersive X-ray spectroscopy (EDS) measurements were carried out on ultrahigh resolution field emission scanning electron microscope (JSM-7600 F), operating at an accelerating voltage of 10 kV. X-ray photoelectron spectroscopy (XPS) measurements were recorded on a Thermo VG Scientific ESCALAB 250XI electron spectrometer with a monochromatic Al Kα X-ray source (1486.6 eV photons). Hydrodynamic diameter measurements of GSH-CGS/ZnS QDs were recorded on a dynamic light scatter (DLS, Malvern NANO-ZS920).

2.3. Synthesis of CGS/ZnS QDs

CGS/ZnS QDs were prepared according to previously reported procedures with a slight change [24]. $Cu(Ac)_2$ (0.5 mmol), ($Ga(NO_3)_3{\cdot}xH_2O$ (0.5 mmol) and 5 mL of OLA were added into a three-neck flask reactor and degassed under vacuum at 140 ℃ for 30 min. Keep this temperature, 0.5 mL of DDT was quickly injected into the reactor. The mixture was then heated to 180 ℃ under an argon atmosphere. After that, 2 mmol S powder was dispersed in 2 mL of ODE at 190 ℃, and then swiftly added into the reactor at 180 ℃ for 10 min. Subsequently, the solution which consisted of 4 mmol $Zn(Ac)_2$, 2 mL of DDT, 2 mL of ODE and 4 mL of OA, was slowly introduced into the above solution and then the mixture was held at 230 ℃ for 2 h. The resulting oil phase products were purified after cooling by precipitation in ethanol and cyclohexane.

2.4. Hydrophilic modification of CGS/ZnS QDs by ligand exchange

Typically, 20 mg of the dried CGS/ZnS QDs, 200 mg GSH, 2 mL MPA and 3 mL DMF were mixed into a flask reactor. Then, the mixture was stirred under the protection of argon at 130 ℃ for 45 min. After that, the outcome GSH-CGS/ZnS QDs solution was washed by methanol, and finally dispersed in water.

2.5. IFE-based fluorescent detection of ALP

10 μL of ALP with an activity ranging from 0 to 100 U L^{-1} was introduced into Tris-HCl buffer solution (pH 7.4), which consisted of 0.1 μM $MgSO_4$ and 1 mM PNPP. Then the mixed solution was incubated at 37 ℃ for 30 min, after that, 1 mL of GSH-CGS/ZnS QDs solution was injected, and the fluorescence spectra at an excitation wavelength of 400 nm was investigated.

2.6. Cell imaging and cytotoxicity assays

The human breast cancer cells of MCF-7 were acquired from the cell bank of Chinese Academy of Sciences (Shanghai, China) and cultured at 37 ℃ in high glucose DMEM supplemented with 10 % Fetal Bovine Serum (FBS) in a 5% CO_2 environment. In a typical assay, GSH-CGS/ZnS QDs (200 μg mL^{-1}) were added into cell and incubated for 30 min. Next, the GSH-CGS/ZnS QDs loaded cells were washed several times and then PNPP (1 mM) was introduced into cells with an incubation time of 1 h and 2 h, respectively. After each indicated time interval incubation, the plates containing cells were taken out and rinsed by sterile PBS several times, and then fresh serum free medium was added. Fluorescent images of cells were obtained by a confocal microscope.

The cytotoxicity of the GSH-CGS/ZnS QDs was estimated by 3-(4,5-dimethylthiazol-2-yl)-2,5-diphenyltetrazolium bromide (MTT) method. MCF-7 cells were firstly incubated with GSH-CGS/ZnS QDs for 24 h in 96-well plates, MTT solution (5 mg mL^{-1}) was introduced to each well and incubated for 4 h. Finally, dimethylsulfoxide (DMSO, 100 μL) was injected into each well. The cytotoxic effect of the GSH-CGS/ZnS QDs was evaluated through the absorbance ratio of the GSH-CGS/ZnS QDs treated sample versus the control sample.

3. Results and discussion

3.1. Preparation and characterization of CGS/ZnS QDs

The synthetic process was in accordance with the literature with slight modification [24]. The oil-soluble CGS/ZnS QDs were transformed into water-soluble by ligand exchange with MPA and GSH. TEM image showed that CGS/ZnS QDs in cyclohexane were about 7 − 8 nm (Fig. S1). After ligand exchange, the GSH-CGS/ZnS QDs were well separated (Fig. 1(a)). Fig. 1(b) showed the results of the Dynamic light scattering (DLS) measurements. The hydrodynamic diameter of GSH-CGS/ZnS QDs was about 10 nm and very uniform.

XRD patterning showed that the CGS/ZnS nanocrystals matched with the patterns of $CuGaS_2$ (JCPDS card No. 25-0279) and ZnS (JCPDS card No. 77-2100) with well crystallization, respectively (Fig. 2(a)). EDS measured data also confirmed that the black nanocrystals were composed of Cu, Ga, Zn and S elements with a molar ratio of Cu : Ga approaching 1:1 (Fig. 2(b)). To further clarify the structure and composition of CGS/ZnS QDs, the high-resolution XPS spectra were recorded in Fig. S2(a). The binding energy located at 932.5 and 952.2 eV in Fig. S2(b), which attributed to the Cu 2p3/2 and Cu 2p1/2 of Cu (I), respectively. The XPS peaks at 1119.2 and 1142.3 eV respectively from Ga 2p3/2 and 2p1/2 of CGS/ZnS QDs in Fig. S2(c), indicating the

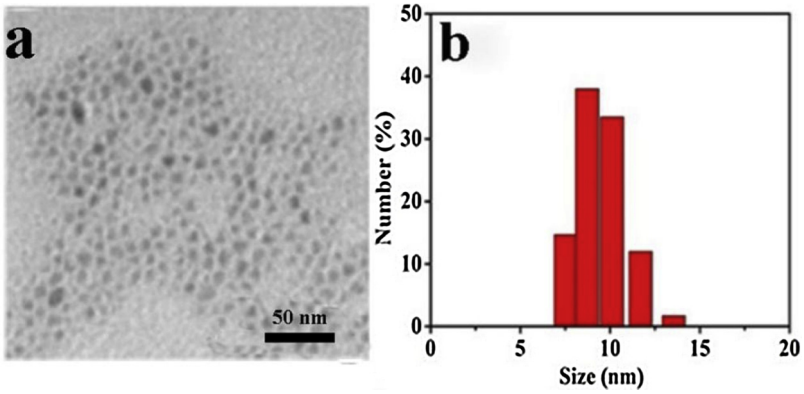

Fig. 1. TEM micrograph (a) GSH-CGS/ZnS QDs. (b) The DLS measurement of GSH-CGS/ZnS QDs.

presence of Ga (III). The peaks showed at 161.4 and 162.3 eV in Fig. S2(d) should be assigned to the S 2p3/2 and 2p1/2 peak, respectively. The above results proved the successful synthesis of CGS/ZnS QDs.

Furthermore, the fluorescence spectra of the initial oil phase CGS/ZnS and the resulting water-soluble GSH-CGS/ZnS QDs were shown in Fig. 3(a). The maximum excitation of GSH-CGS/ZnS QDs was at 400 nm, and a corresponding emission was observed at 601 nm. Compared to the oil phase CGS/ZnS, the emission peak had a tiny shift from 592 to 601 nm. The slight shift of emission peak can probably be attributed to the moderate growth of the QDs after phase transfer [35]. From Fig. 3(a) (insert 1, 2), it can be clearly seen that the QDs were successfully transferred into aqueous phase, which showed yellow fluorescence under the irradiation of an ultraviolet lamp.

QDs were dispersed in water and deposition was not observed after one week of storage at 4 ℃. Moreover, the fluorescence intensity of GSH-CGS/ZnS QDs had no significant change (Fig. 3b). Results indicated the fluorescence stability of GSH-CGS/ZnS QDs was well maintained, which the fluorescence property of samples is very important for their bioimaging application within the experimental conditions.

The ligand exchange of the GSH-CGS/ZnS QDs was investigated by FTIR (Fig. S3(a)). After ligand exchange, it was found that QDs had an obvious sharp band at 1698 cm^{-1}, which could be attributed to the C=O vibration from GSH [35]. For comparison, there was no obvious peak at the same place in the FTIR spectrum of the CGS/ZnS QDs. Result indicated ligand exchange was successfully performed on the surface of QDs. As shown in Fig. S3(b), the GSH- CGS/ZnS QDs had zeta potential of -12.2 mV in deionized water, which was in consistent with the presence of a carboxyl group on their surface [35].

3.2. Detection of ALP activity by GSH-CGS/ZnS QDs based on inner filter effect

Based on IFE principle, a simple and sensitive fluorescent assay for ALP detection was proposed (Scheme 1). For the detection purpose, the GSH-CGS/ZnS QDs were selected as fluorometric reporters, and PNPP was chosen as ALP substrate, which can be catalytically converted to PNP by ALP. It can be seen from Fig. S4 that the UV–vis absorption peak of PNPP was at 304 nm. However, PNP had a strong absorption peak at 405 nm, which overlapped with the fluorescence excitation spectrum of the GSH-CGS/ZnS QDs. Therefore, PNP might induce the fluorescence quenching of GSH-CGS/ZnS QDs through IFE. Based on this, the concentration of ALP had a quantitative relationship with the fluorescence intensity of GSH-CGS/ZnS QDs.

The UV absorption spectra of the ALP reaction systems with different ALP concentrations from 0 to 100 U L^{-1} were recorded (Fig. 4). With the adding ALP concentration increased, the absorption intensity of PNPP (at 304 nm) were gradually weakened and the absorption intensity of PNP (at 405 nm) were gradually enhanced. Furthermore, PNPP had a maximum UV absorbance at 304 nm, which had no effect on the excitation of GSH-CGS/ZnS QDs. It indicated that using GSH-CGS/ZnS QDs as fluorometric reporter would not interfere with the detection results of ALP.

As shown in Fig. S5, the fluorescence of GSH-CGS/ZnS QDs remained unchanged when PNPP was introduced alone. However, when ALP and PNPP were added simultaneously, PNPP can be catalytically hydrolyzed to PNP, resulting in the fluorescence quenching of the GSH-CGS/ZnS QDs. In addition, we also tested whether the presence of Na^+, K^+, Cl^-, and L-Cysteine would affect the detection of ALP. It can be seen from Fig. S5(b) that there was no effect on the detection of ALP when Na^+, K^+, Cl^-, and L-Cysteine was added respectively.

Further, different concentrations of ALP were introduced to 1 mL GSH-CGS/ZnS QDs solution and incubated with PNPP, after that their fluorescence was monitored. As shown in Fig. 5(a), the fluorescence emission of GSH-CGS/ZnS QDs did not change when ALP was not added into GSH-CGS/ZnS QDs solution incubated PNPP. After adding ALP into the solution, the fluorescence intensity of the GSH-CGS/ZnS decreased. Regularly decreased fluorescence intensities of GSH-CGS/ZnS QDs were

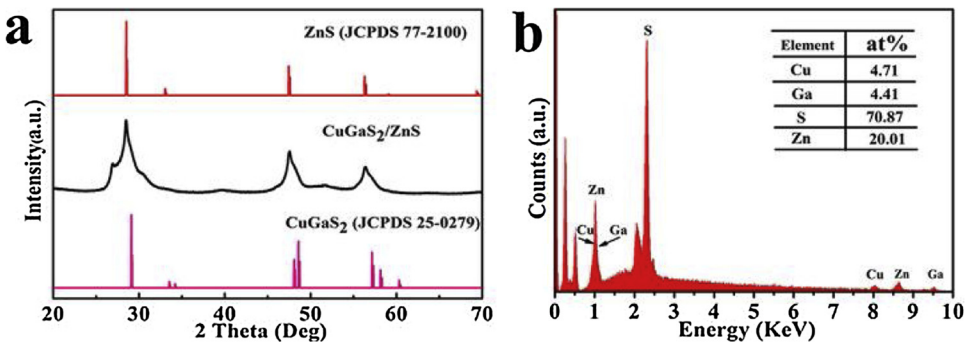

Fig. 2. (a) XRD and (b) EDS spectra of CGS/ZnS QDs.

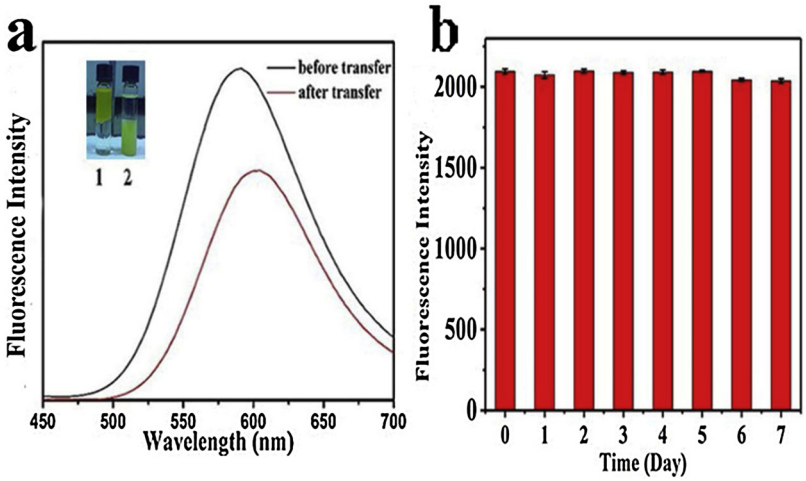

Fig. 3. (a) Fluorescence spectra of CGS/ZnS QDs before and after ligand exchange. (Insert: 1: Photographs of samples CGS/ZnS QDs in cyclohexane under UV light; 2: Photographs of samples GSH-CGS/ZnS QDs in water under UV light); (b) The colloidal stability of hydrophilic GSH-CGS/ZnS QDs at 4 ℃ for a week storage (SD, n = 3).

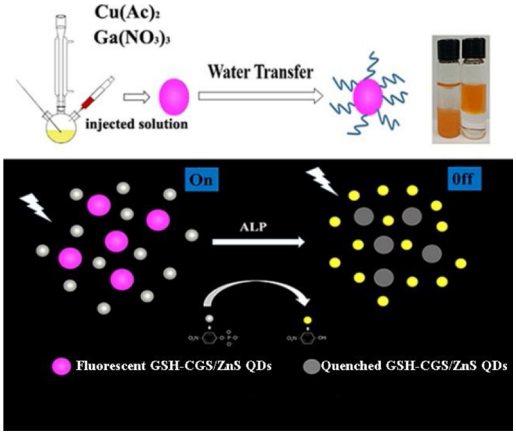

Scheme 1. Specific detection process of ALP based on inner filter effect.

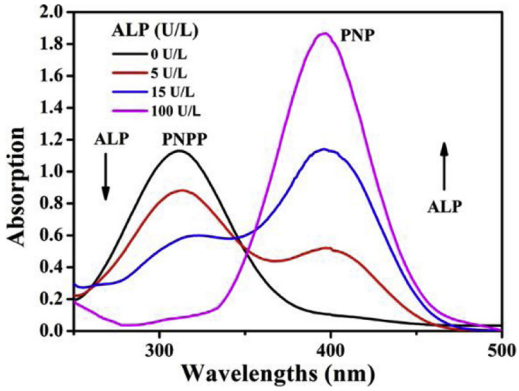

Fig. 4. The changes of absorption spectra of PNPP (at 304 nm) and PNP (at 405 nm) with presence of ALP.

recorded after adding different concentrations of ALP from 0 to 100 U L^{-1}. In the inset of Fig. 5(b), a good linear relationship was obtained between the relative fluorescence intensity (F_0 –F) and the ALP concentration in the range of 0.05–10 U L^{-1}, where F_0 and F are the fluorescence intensity of the GSH-CGS/ZnS QDs in the absence and presence of ALP, respectively. The liner fitting equation can be expressed as follows:

$$F_0 - F = 101.23[ALP] + 140.297,\ U\ L^{-1}$$

The corresponding linear correlation coefficient was 0.98, and the detection limit of ALP was as low as 0.01 U L^{-1} on the basis of 3δ/k (where δ is the standard deviation of the blank signal and k is the slope of the calibration curve), which was much lower than most of other methods (Table 1).

3.3. Selectivity study

Selectivity is an important parameter for evaluating biosensor. To investigate the specificity of the sensor based on GSH-CGS/ZnS QDs for ALP, the PL emission effects of the sensor to proteins and enzymes (including trypsin, immunoglobulin G (IgG), Glucose oxidase(GOx), lysozyme, bull serum albumin (BSA), human serum albumin (HAS) and phosphatase (1- (Prop-2-yn-1-yloxy) propan-2-ol(acid phosphatase, AP)) were studied.

The values of fluorescence intensity ratio F/F_0 of the GSH-CGS/ZnS QDs in the absence and presence of proteins, enzymes biomarker and acid phosphatase were presented in Fig. 6. The results showed that no any protein biomarker except ALP, which can significantly reduce the F/F_0 value, indicating that the sensor had high selectivity for ALP. The high selectivity of the sensor we proposed was mainly attributed to the specificity catalysis of ALP to PNPP. In other words, the presence of trypsin, IgG, GOx, lysozyme, BSA, HAS and AP did not affect the fluorescent detection of GSH-CGS/ZnS QDs.

3.4. Fluorescence imaging in living cells

The cytotoxicity of GSH-CHS/ZnS QDs was assessed by MTT assay for bioimaging application. Results indicated that the toxicity of GSH-CGS/ZnS QDs to MCF-7 cells was not significant compared with the control group (Fig. S6), even at high concentration (300 μg mL^{-1}). In addition, PNPP has not cytotoxicity, which has been proved by relevant literature [41].

In order to further demonstrate the application of the sensor in biological system, we used ALP-overexpressed MCF-7 cells to evaluate the cell imaging ability of the GSH-CGS/ZnS QDs probe. Fig. S7 showed the confocal brightfield images and the corresponding confocal fluorescence images in MCF-7 cells incubated with GSH-CGS/ZnS QDs. Firstly, MCF-7 cells were incubated with GSH-CGS/ZnS QDs for 30 min. The imaging of intracellular ALP was shown in Fig. S7(a) and (b). MCF-7 cells without PNPP showed strong fluorescence under laser confocal illumination. Then, with the time of the QDs-loaded cells incubated with 1 mM PNPP was prolonged to 1 h and 2 h respectively, more PNPP was hydrolyzed to PNP by ALP (Fig. S7(c)-(f)). Based on the IFE, only the fluorescence of the cell itself was observed after the prolonged time (Fig. S7(f)). The results clearly demonstrated that the probe we proposed could offer the potential for sensitive detection of ALP.

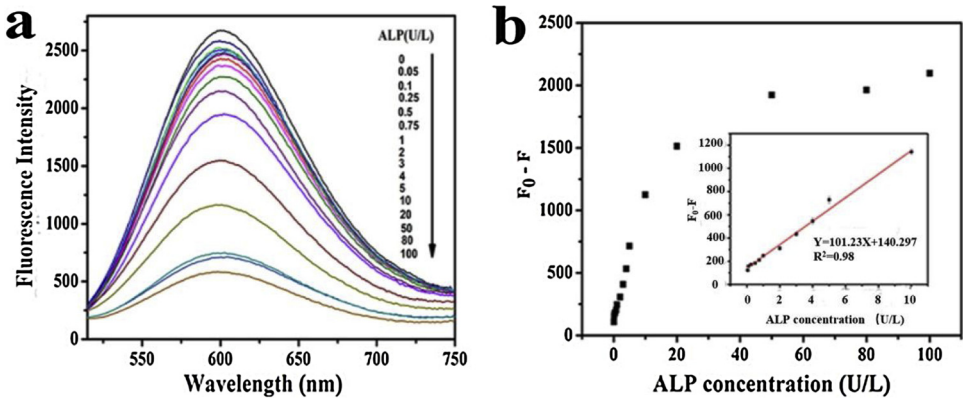

Fig. 5. (a) The emission intensity of GSH-CGS/ZnS QDs changes at different ALP concentrations (from top to bottom 0, 0.05, 0.1, 0.25, 0.5, 0.75, 1, 2, 3, 4, 5, 10, 20, 50, 80 and 100 U L^{-1}) with 1 mM PNPP incubated at 37 ℃ for 30 min. (b) Plots of (F_0 –F) versus ALP concentrations from 0 to 100 U L^{-1} (insert: its corresponding liner relationship from 0.05 to 10 U L^{-1}). F_0 and F are the fluorescence intensities of CGS/ZnS QDs in the absence and presence of ALP, respectively (SD, n = 3).

Table 1
The sensitivity comparison of various analytical measures for detection of ALP.

Methods	Linear range (U L^{-1})	LOD (U L^{-1})	References
Ti_3C_2 QDs	0.1–2	0.02	[37]
Hemin/G-quadruplex	0.1–5	0.03	[38]
MoS_2 QDs	0–5	0.1	[39]
VS_2 QDs	3.0–1000	0.27	[40]
$CuGaS_2$/ZnS	0.05–10	0.01	This work

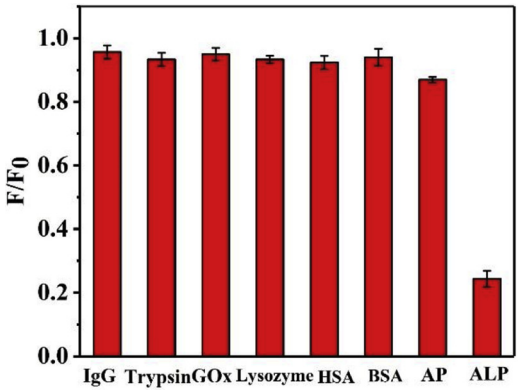

Fig. 6. Intensity ratio F/F_0 of PL emission peak intensities of the biosensor to different protein and enzymes biomarkers (Including trypsin, IgG, GOx, lysozyme, BSA, HAS and AP) (SD, n = 3).

4. Conclusions

In this case, the water-soluble CGS/ZnS QDs obtained by efficient ligand exchange with MPA and GSH could exhibit well-dispersed, good stability and bright PL emission. The fluorescence intensity of GSH-CGS/ZnS QDs can be significantly quenched by the conversion of PNPP to PNP with the specific catalysis of ALP. Therefore, based on the IFE, the hydrophilic GSH-CGS/ZnS QDs we synthesized were successfully applied in the biomedical field for ALP detection, showing the advantages of high sensitivity and selectivity.

CRediT authorship contribution statement

Xiaoxia Huangfu: Investigation, Data curation, Writing - original draft. **Yang Shen:** Investigation, Data curation, Methodology. **Anzi Yang:** Visualization, Investigation. **Lixiao Liu:** Data curation. **Wen Luo:** Software, Validation. **Wenbo Zhao:** Conceptualization, Methodology, Writing - review & editing.

Declaration of Competing Interest

The authors have declared no conflict of interest.

Acknowledgments

This work was supported by National and Local Joint Engineering Research Center of Biomedical Functional Materials, Jiangsu Key Laboratory of Biofunctional Materials, Projects of Jiangsu Collaborative Innovation Center of Biomedical Functional Materials, National Natural Science Foundation of China (21571104).

Appendix A. Supplementary data

Supplementary material related to this article can be found, in the online version, at doi:https://doi.org/10.1016/j.colsurfb.2020.110984.

References

[1] X. Michalet, F.F. Pinaud, L.A. Bentolila, J.M. Tsay, S. Doose, J.J. Li, G. Sundaresan, A.M. Wu, S.S. Gambhir, S. Weiss, Quantum dots for live cells, in vivo imaging, and diagnostics, Science 307 (2005) 538–544.
[2] G. Xu, S. Zeng, B. Zhang, M.T. Swihart, K.-T. Yong, P.N. Prasad, New Generation Cadmium-Free Quantum Dots for Biophotonics and Nanomedicine, Chem. Rev. 116 (2016) 12234–12327.
[3] K.D. Wegner, N. Hildebrandt, Quantum dots: bright and versatile in vitro and in vivo fluorescence imaging biosensors, Chem. Soc. Rev. 44 (2015) 4792–4834.
[4] D. Jaque, C. Richard, B. Viana, K. Soga, X.G. Liu, J.G. Sole, Inorganic Nanoparticles for Optical Bioimaging, Adv. Opt. Photonics 8 (2016) 1–103.
[5] C.H. X, J.D. Meeldijk, H.C. Gerritsen, Highly luminescent water-dispersible NIR-emitting wurtzite $CuInS_2$/ZnS core/shell colloidal quantum dots, Chem. Mater. 29 (2017) 4940–4951.
[6] P.D. Howes, R. Chandrawati, M.M. Stevens, Colloidal nanoparticles as advanced biological sensors, Science 346 (2014) 53–63.
[7] F.M. Winnik, D. Maysinger, Quantum dot cytotoxicity and ways to reduce it, Acc. Chem. Res. 46 A (2013) 672–680.
[8] R. Marin, A. Vivian, A. Skripka, A. Migliori, V. Morandi, F. Enrichi, F. Vetrone, P. Ceroni, C. Aprile, P. Canyon, Mercaptosilane-passivated $CuInS_2$ quantum dots for luminescence thermometry and luminescent labels, ACS Appl. Nano Mater. 2 (2019) 2426–2436.
[9] T. Pons, E. Pic, N. Lequeux, E. Cassette, L. Bezdetnaya, F. Guillemin, F. Marchal, B. Dubertret, Cadmium-Free $CuInS_2$/ZnS Quantum Dots for Sentinel Lymph Node Imaging with Reduced Toxicity, ACS Nano 4 (2010) 2531–2538.
[10] J.Y. Zhao, G. Chen, Y.P. Gu, R. Cui, Z.L. Zhang, Z.L. Yu, B. Tang, Y.F. Zhao, D.W. Pang, Ultrasmall Magnetically Engineered Ag_2Se Quantum. Dots for Instant Efficient Labeling and Whole-Body High-Resolution Multimodal Real-Time Tracking of Cell-Derived Microvesicles, J. Am. Chem. Soc. 138 (2016) 1893–1903.
[11] J.Y. Chang, G.Q. Wang, C.Y. Cheng, W.X. Lin, J.C. Hsu, Strategies for Photoluminescence Enhancement of $AgInS_2$Quantum Dots and Their Application as Bioimaging Probes, J. Mater. Chem. 22 (2012) 10609–10618.
[12] Y.B. Yang, L. Lin, L.J. Jing, X.L. Yue, Z.F. Dai, $CuInS_2$/ZnS Quantum Dots Conjugating Gd(III) Chelates for Near-Infrared Fluorescence and Magnetic Resonance Bimodal Imaging, ACS Appl. Mater. Interfaces 9 (2017) 23450–23457.
[13] J. Park, C. Dvoracek, K.H. Lee, J.F. Galloway, H.E.C. Bhang, M.G. Pomper, P.C. Searson, CuInSe/ZnS Core/Shell NIR Quantum Dots for Biomedical Imaging, Small 7 (2011) 3148–3152.
[14] C. Coughlan, M. Ibanez, O. Dobrozhan, A. Singh, A. Cabot, K.M. Ryan, Compound copper chalcogenide nanocrystals, Chem. Rev. 117 (2017) 5865–6109.
[15] K.E. Knowles, K.H. Hartstein, T.B. Kilburn, A. Marchioro, H.D. Nelson,

P.J. Whitham, D.R. Gamelin, Luminescent Colloidal Semiconductor Nanocrystals Containing Copper: Synthesis, Photophysics, and Applications, Chem. Rev. 116 (2016) 10820–10851.
[16] J. Tang, S. Hinds, S.O. Kelley, E.H. Sargent, Synthesis of Colloidal $CuGaSe_2$, $CuInSe_2$, and $Cu(InGa)Se_2$ Nanoparticles, Chem. Mater. 20 (2008) 6906–6910.
[17] Y.H.A. Wang, X.Y. Zhang, N.Z. Bao, B.P. Lin, A. Gupta, Synthesis of Shape-Controlled Monodisperse Wurtzite $CuIn_xGa_{1-x}S_2$ Semiconductor Nanocrystals with Tunable Band Gap, J. Am. Chem. Soc. 133 (2011) 11072–11075.
[18] M. Jalalah, M.S. Assiri, J.G. Park, One-Pot Gram-Scale, Eco-Friendly, and Cost-Effective Synthesis of $CuGaS_2$/ZnS Nanocrystals as Efficient UV-Harvesting Down-Converter for Photovoltaics, Adv. Energy Mater. 8 (2018) 1703418.
[19] S. Das Adhikari, A. Dutta, G. Prusty, P. Sahu, N. Pradhan, Symmetry break and seeded 2D anisotropic growth in ternary $CuGaS_2$ nanocrystals, Chem. Mater. 29 (2017) 5384–5393.
[20] S.H. Chang, B.C. Chiu, T.L. Gao, S.L. Jheng, H.Y. Tuan, Selective synthesis of copper gallium sulfide ($CuGaS_2$) nanostructures of different sizes, crystal phases, and morphologies, CrystEngComm 16 (2014) 3323–3330.
[21] M.S. Zhao, F. Huang, H. Lin, J.C. Zhou, J. Xu, Q.P. Wu, Y.S. Wang, $CuGaS_2$-ZnS p-n Nanoheterostructures: A Promising Visible Light Photo-catalyst for Water-splitting Hydrogen Production, Nanoscale 8 (2016) 16670–16676.
[22] D.Y. Jo, D. Kim, J.H. Kim, H. Chae, H.J. Seo, Y.R. Do, H. Yang, Tunable White Fluorescent Copper Gallium Sulfide Quantum Dots Enabled by Mn Doping, ACS Appl. Mater. Interfaces 8 (2016) 12291–12297.
[23] D.Y. Jo, H. Yang, Synthesis of highly white-fluorescent Cu-Ga-S quantum dots for solid-state lighting devices, Chem. Commun. 52 (2016) 709–712.
[24] J.H. Kim, D.Y. Jo, K.H. Lee, E.P. Jang, C.Y. Han, J.H. Jo, H. Yang, White electroluminescent lighting device based on a single quantum dot emitter, Adv. Mater. 28 (2016) 5093–5098.
[25] J.A. Lorente, H. Valenzuela, J. Morote, A. Gelabert, Serum bone alkaline phosphatase levels enhance the clinical utility of prostate specific antigen in the staging of newly diagnosed prostate cancer patients, Eur. J. Nucl. Med. 26 (1999) 625–632.
[26] J.M. Liu, M.L. Cui, X.X. Wang, L.P. Lin, L. Jiao, L.H. Zhang, Z.Y. Zheng, L.Z. Huang, Highly selective affinity adsorption imprinting phosphorescence sensor for determination of trace alkaline phosphatase and prediction of human diseases, Sens. Actuators B-Chem. 186 (2013) 521–527.
[27] N.J. Fernandez, B.A. Kidney, Alkaline phosphatase: beyond the liver, Vet. Clin. Path. 36 (2007) 223–233.
[28] J.H. Zhao, S. Wang, S.S. Lu, X.F. Bao, J. Sun, X.R. Yang, An Enzyme Cascade-Triggered Fluorogenic and Chromogenic Reaction Applied in Enzyme Activity Assay and Immunoassay, Anal. Chem. 90 (2018) 7754–7760.
[29] L. He, H.W. Yang, P.F. Xiao, R. Singh, N.Y. He, B. Liu, Z.Y. Li, Highly Selective, Sensitive and Rapid Detection of Escherichia coli O157: H7 Using Duplex PCR and Magnetic Nanoparticle-Based Chemiluminescence Assay, J. Biomed. Nanotechnol. 13 (2017) 1243–1252.
[30] J. Dong, Y. Li, M.Y. Zhang, Z. Li, T.Y. Yan, W.P. Qian, Ultrasensitive surface-enhanced Raman scattering detection of alkaline phosphatase, Anal. Methods 6 (2014) 9168–9172.
[31] L. Yang, M.X. Gao, L. Zhan, M. Gong, S.J. Zhen, C.Z. Huang, An Enzyme-induced Au@Ag Core-shell NanoStructure Used for an Ultrasensitive Surface-enhanced Raman Scattering Immunoassay of Cancer Biomarkers, Nanoscale 9 (2017) 2640–2645.
[32] W.J. Zhang, H.X. Yang, N. Li, N. Zhao, A sensitive fluorescent probe for alkaline phosphatase and an activity assay based on the aggregation-induced emission effect, RSC Adv. 8 (2018) 14995–15000.
[33] F.L. Qu, H.M. Pei, R.M. Kong, S.Y. Zhu, L. Xia, Novel Turn-on Fluorescent Detection of Alkaline Phosphatase Based on Green Synthesized Carbon Dots and MnO_2Nanosheets, Talanta 165 (2017) 136–142.
[34] C.S. Park, T.H. Ha, M. Kim, N. Raja, H.S. Yun, M.J. Sung, O.S. Kwon, H. Yoon, C.S. Lee, Fast and sensitive near-infrared fluorescent probes for ALP detection and 3d printed calcium phosphate scaffold imaging in vivo, Biosens. Bioelectron. 105 (2018) 151–158.
[35] C.Z. Zhao, Z.L. Bai, X.Y. Liu, Y.J. Zhang, B.S. Zou, H.Z. Zhong, Small GSH-Capped $CuInS_2$Quantum Dots: MPA-Assisted Aqueous Phase Transfer and Bioimaging Applications, ACS Appl. Mater. Interfaces 7 (2015) 17623–17629.
[36] J.Y. Zhang, X.M. Lu, Y. Lei, X.D. Hou, P. Wu, Exploring the tunable excitation of QDs to maximize the overlap with the absorber for inner filter effect-based phosphorescence sensing of alkaline phosphatase, Nanoscale 9 (2017) 15606–15611.
[37] Z. Guo, X.H. Zhu, S.G. Wang, Y. Huang, Z. Nie, S.Z. Yao, Fluorescent Ti_3C_2MXene Quantum Dots for an Alkaline Phosphatase Assay and Embryonic Stem Cell Identification Based on the Inner Filter Effect, Nanoscale 10 (2018) 19579–19585.
[38] Y.Q. Liu, E.H. Xiong, X.Y. Li, J.J. Li, X.H. Zhang, J.H. Chen, Sensitive Electrochemical Assay of Alkaline Phosphatase Activity Based on TdT-mediated Hemin/G-quadruplex DNAzyme Nanowires for Signal Amplification, Biosens. Bioelectron. 87 (2017) 970–975.
[39] Y.P. Zhong, F.F. Xue, P. Wei, R.H. Li, C.Y. Cao, T. Yi, Water-soluble MoS_2 quantum dots for facile and sensitive fluorescence sensing of alkaline phosphatase activity in serum and live cells based on the inner filter effect, Nanoscale 10 (2018) 21298–21306.
[40] X.H. Ma, C.C. Du, M.X. Shang, W.B. Song, VS_2Quantum Dot Label-free Fluorescent Probe for Sensitive and Selective Detection of ALP, Anal. Bioanal. Chem. 410 (2018) 1417–1426.
[41] A. Hiroshi, H.C. Marcela, F. Veríssima, Relationship Between Phosphatase Activity and Cytotoxic Effect of Two Protein Phosphatase Inhibitors, Okadaic Acid and Pervanadate, on Human Myeloid Leukemia Cell Line, Enzym. Inhib. Med. Chem. 18 (2003) 425–429.